CHAPTER 3

IDENTIFICATION OF CHLOROGENIC ACID BY *IN SILICO* SCREENING OF *WITHANIA SOMNIFERA* PHYTOCHEMICALS AS A POTENT INHIBITOR FOR NMDAR, NNOS/INOS AND MMP-2/9

Highlights of the Chapter

- *A set of 40 phytochemicals of Withania somnifera were evaluated for their suitability of drug likeness and ability to penetrate the blood brain barrier*
- *25 phytochemicals qualify the criteria of drug likeness and BBB penetration were docked near the active/catalytic site of NMDAR, nNOS/iNOS and MMP-2/9*
- *Chlorogenic acid appeared as a potent multi-target inhibitor as it displayed extensive hydrogen bounding and hydrophobic interaction with all molecular targets compared to their inhibitors.*

Abstract

Cerebral ischemia occurs due to occlusion in blood vessels that supply oxygen and glucose to the nerve cells. Interruption in cerebral blood flow leads to ATP production failure, disruption in ion homeostasis and loss of electrical activity. These phenomena leads to activation/overexpression of NMDARs, nNOS, iNOS, MMP-2 and MMP-9 that triggers a complex cascade of detrimental physiological and biochemical events resulting in neuronal cell death. Due to least efficacy and side effects of synthetic inhibitors of these molecular mediators of neuronal dysfunction, identification of a potent phytochemical as multi-target inhibitor that may act as neurotherapeutic agent to combat the cerebral ischemic insult is an active area of research. *Withania somnifera* (WS) has been used as a nootropic agents and nerve tonic for centuries in Ayurveda. The present structural-based *in silico* study was carried out to search potent inhibitor for NMDARs, nNOS, iNOS, MMP-2 and MMP-9. Forty WS phytochemicals were evaluated for their BBB penetration ability, mutagenicity, druglikeness

and Human Intestinal Absorption properties. 25 phytochemicals qualify the criteria of drug likeness and BBB penetration were selected for the molecular docking study with protein targets. Results reveled that chlorogenic acid consistently displayed higher affinity toward these protein targets by forming higher hydrogen bonding and establishing hydrophobic interactions with active/catalytic site residues critical in mediating inhibition of NMDAR, nNOS, iNOS, MMP-2 and MMP-9.

3.1 INTRODUCTION

The NMDA receptors play essential roles in the transmission, integration and plasticity of excitatory signals and are crucial for higher functions of the mammalian central nervous system [135]. Structurally they are heterotetramers, typically containing two glycine or D-serine binding GluN1 subunits and two L-glutamate binding GluN2 subunits [136]. The obligate GluN1 subunit, encoded by a single gene, can exist in eight isoforms (GluN1-1a to GluN1-4a, and, GluN1-1b to GluN1-4b) and influence the properties of the channel. Also, four separate genes encode four different GluN2 subunits (GluN2A-D) [137]. The most extensively expressed NMDARs contain the obligate subunit GluN1 plus either GluN2B or GluN2A or a mixture of the two. However, a recent study has reported that GluN2B-containing NMDARs tend to promote neuronal death, irrespective of location (synaptic or extrasynaptic) while GluN2Acontaining NMDARs promote survival [138]. Neuronal death occurs when neurons get prolonged exposure to glutamate resulting overactivation of NMDARs that are highly permeable for Ca^{2+}. High Ca^{2+} influx through the NMDA receptors triggers many intracellular events that lead to neuronal death, as illustrated in Fig. 3.1.

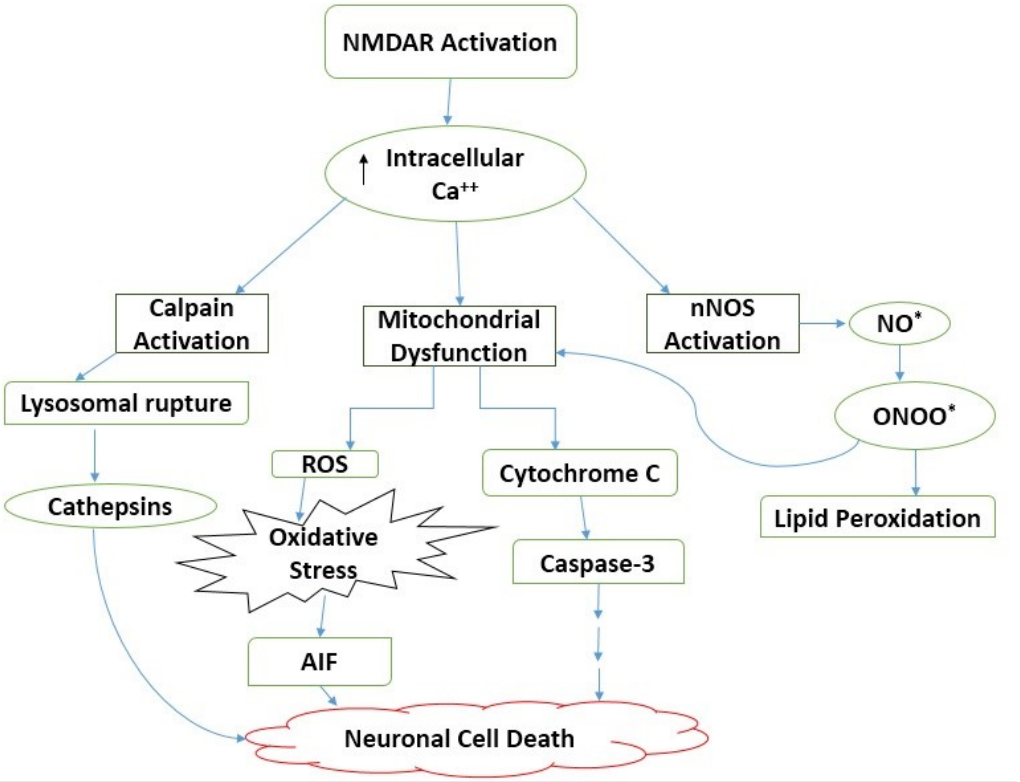

Fig. 3.1 NMDARs mediated excitotoxicity resulting neuronal cell death [139]. Activation of NMDARs leading to intracellular calcium overloads resulting activation of calpain, neuronal nitric oxide synthase (nNOS) and mitochondrial oxidative stress. Calpain activation engaging both cathepsins and calpain-dependent cell death. Activation of nNOS leading to peroxynitrite production that causes lipid peroxidation and mitochondrial dysfunction. Leakage of cytochrome C- an inner mitochondrial membrane protein into the cytosol activates caspase-3 resulting neuronal cell death. Formation of reactive oxygen species (ROS) causes oxidative stress leading to production of apoptosis inducing factors (AIF) which promote apoptotic cell death.

There is evidence that GluN2B-containing NMDARs precipitate neurodegeneration in various neurological diseases, like Huntington's disease [140], Parkinson's disease [141], Alzheimer's disease [142], traumatic brain injury [143], multiple sclerosis [144], Epilepsy [145], Cerebral ischemia [146], Amyotrophic lateral sclerosis [147] and schizophrenia [148]. Therefore, considerable effort has been directed toward the development of clinically useful GluN2B-selective NMDA receptor antagonists [149][150]. Williams (1993) reported that Ifenprodil (a kind of phenylethanolamine compound) inhibits GluN1/GluN2B receptors with a 400-fold

selectivity over the other GluN2 subunits [151]. Further studies indicated that Ifenprodil's subunit-selectivity is controlled by the GluN2B amino-terminal domain (ATD) [152] and Ifenprodil binds at the interface of GluN1 and GluN2B ATD heterodimer in a subtype-specific manner rather than within a cleft of the bilobed ATD (Fig. 3.2) [153]. These studies provide a molecular blueprint for searching and designing of therapeutic compounds targeting the ATD of the NMDA receptor. Nevertheless, due to lack of efficacy and adverse effects of NMDA receptor antagonists to prevent brain injury, clinical trials in human are still disappointing. The clinical trial of Ifenprodil in humans for stroke was abandoned because of high risk/benefits ratio arising from adverse cardiovascular consequences at higher doses [154].

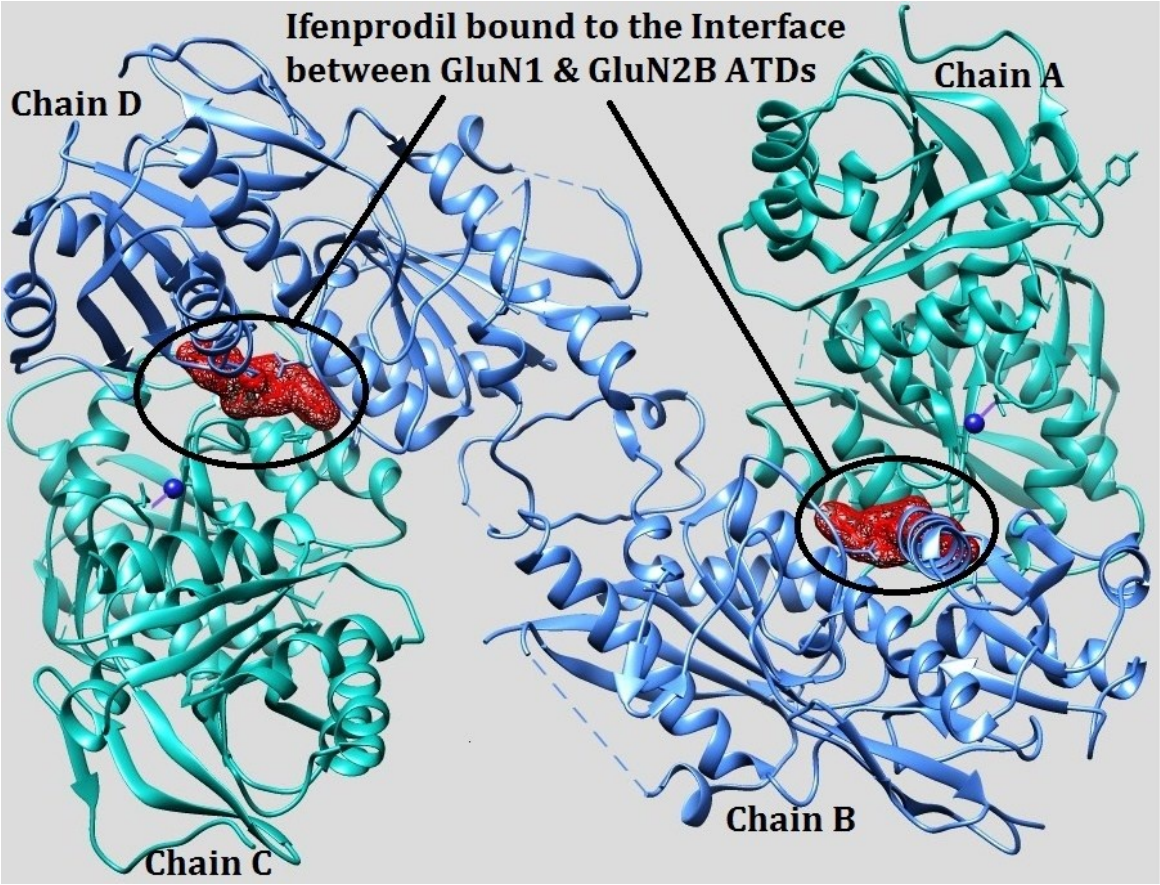

Fig. 3.2 Rounded ribbon structure of NMDA amino-terminal domains (ATD) having two subunits: GluN1b (light sea green) and GluN2B (cornflower blue), in complex with Ifenprodil (red mesh surface). (Visualization with the UCSF Chimera package v.1.10.2).

Nitric oxide (NO) is an essential neurotransmitter that facilitates many vital physiological functions within the brain, cardiovascular, and immune systems [155]. NO is generated by catalysis from nitric oxide synthases (NOSs) via two consecutive NADPH-dependent monooxygenations [156] (Fig. 3.3). In Mammals, three isoforms of NOSs have been identified: neuronal NOS (nNOS or NOS1), inducible NOS (iNOS or NOS2) and endothelial NOS (eNOS or NOS3) [157]. These nitric oxide synthases shared a similar domain architecture and conserved active site. The N-terminal oxygenase catalytic domain comprising a heme active site and a cofactor site for tetrahydrobiopterin (H4B) that helps to catalyze the conversion of L-arginine to NO and L-citrulline. While the C-terminal reductase domain comprising of FAD, NADPH, and FMN binding sites [158]. For catalysis, NADPH transfers two electrons first to FAD and then to FMN, which transfers one electron to the heme. A calmodulin-binding motif is present in between the oxygenase and reductase domains, which binds calmodulin to enables electron flow from the flavins to the heme (Fig 3.3).

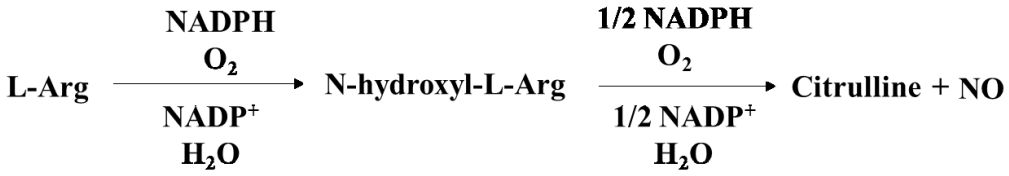

Fig. 3.3 Scheme of the two-step oxygenation of arginine catalyzed by NOSes.

The eNOS and nNOS genes are constitutively expressed. eNOS expression restricted to the endothelium lining of blood vessels. nNOS expressed in CNS, peripheral nervous system (PNS) and some other type of cells. Whereas, expression of iNOS is induced in macrophages and other cell types upon their activation by a wide variety of proinflammatory stimuli [159]. The regulation of nNOS and eNOS are Ca2+/calmodulin-dependent, whereas expression of iNOS is a Ca2+/calmodulin-independent. nNOS and eNOS play a vital role in

neurotransmission and relaxation of smooth muscles respectively, and iNOS is expressed during inflammation, tumor cell cytolysis and bacterial infection. On the other hand, in the face of NO playing beneficial roles, its overproduction has been implicated in numerous pathological situations. In particular, excess NO in the CNS from nNOS activity can lead to many neurological disease states including Alzheimer's disease [160], ischemic stroke [161], Parkinson's disease [162], and migraine [163].

Due to the significance of NO in various neuropathological processes, nNOS are considered as an important pharmacological target [164]. While some nNOS inhibitors have been reported with high affinity, to achieve high selectivity is the major challenging task. Because potent nNOS inhibitors can also inhibit eNOS (plays a vital role in maintaining the vascular tone in the brain) that may cause severe rises in blood pressure [165]. Therefore, dual inhibition of iNOS and nNOS without inhibiting eNOS is a promising neuroprotective approach for combating neurological disorders. Studies suggested that treatment with nNOS and iNOS inhibitors significantly reduced the cerebral infarction in both transient and permanent occlusion rat models [166].

The Gelatinases (MMP-2 and MMP-9) are zinc-dependent endopeptidases play both detrimental and beneficial roles in ischemic insult [167]. The expression of MMP-2 is ubiquitous and it expressed as a 72-kDa proenzyme. It is activated by forming a complex with tissue inhibitor of metalloproteases-2 (TIMP-2) under appropriate stoichiometric conditions [168]. This complex is a substrate for the MMP-14 that converts prodomain of proMMP-2 into 64-kDa active enzyme by proteolytic cleavage (aided by free active MMP-2) [169]. Experimental data suggest that the fully mature 64-kDa active enzyme inhibits neovascularization and induces apoptosis in endothelial cells while 72-kDa proenzyme-TIMP-

2 complex with MMP-14 promotes angiogenesis and enhances cell survival [170]. Differing to MMP-2, MMP-9 is only constitutively expressed in neutrophils. In neutrophils, it is stored in granules and released rapidly after stimulation as a 92-kDa proenzyme [171]. Serine proteases may produce the active form of MMP-9 (83-kDa mature enzyme) by removal of the prodomain or due to disruption of the cysteine switch by oxidative stress. The gelatinases specifically degrade the basal lamina's major components (collagen IV, fibronectin, and laminin) present around the cerebral blood vessels but both are unable to degrade collagen I directly by proteolysis. Under normal conditions, MMPs are expressed in very low to an undetectable level, but their level rises after ischemic stroke [172]. Experimental data clearly demonstrated that after cerebral ischemia, an increase in MMP-2 level (at 3 hours) associated with the initial disruption of the BBB whereas, an increase in MMP-9 level (at 48 hours) related to the delayed opening [173]. Although, Gelatinases play useful roles in the repairing phase in the late stage after cerebral ischemia, including neuronal plasticity, neuroblasts migration and modulating neurovascular remodeling [174]. On the other hand, they play negative roles after cerebral ischemia [175], Hemorrhagic Stroke [176] and perinatal hypoxic-ischemic (HI) brain injury [73]. The possible mechanism of neurodegeneration by activation of MMP-2 and MMP-9 are shown in Figure 3.4. Kinds of literature suggest that combination therapies of gelatinases inhibitor along with tPA can be of therapeutic importance in ischemic stroke. Also, the MMP-2 deficiency in addition to double deficiency of gelatinases were more beneficial than MMP-9 deficiency alone against hemorrhagic transformation (HT) in the initial stages of ischemic insult [177]. Due to the considerable physiological importance of MMPs, as an important therapeutic drug target, it is desirable to find inhibitors that will be selective for gelatinases and not interfere with the normal physiological functions of others [178].

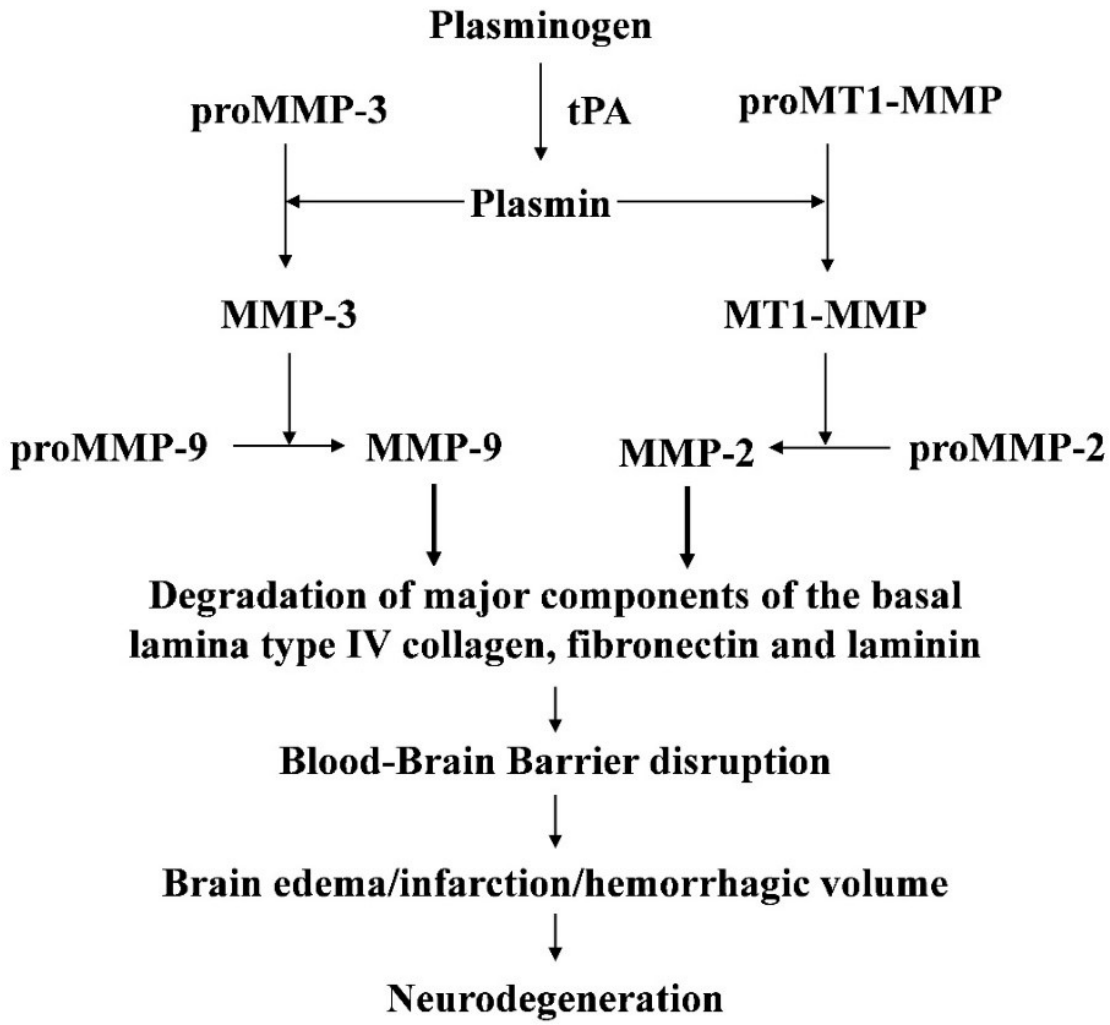

Fig. 3.4 Neurodegeneration through MMP-2 and MMP-9 activation. (Tissue plasminogen activator (tPA) converts the plasminogen into plasmin which further converts pro-membrane type-1 MMP (proMT1-MMP) and ProMMP-3 into MT1-MMP and MMP-3 respectively. MT1-MMP activates the MMP-2 and MMP-3 activate the MMP-9. After stroke free radicals and proinflammatory cytokines production also activate MMP-2 and MMP-9 that leads to degradation of the basal lamina's major components around the blood vessels of the brain including fibronectin, laminin, and collagen IV as well as thereby leads to BBB disruption resulting brain edema, infarction, and hemorrhage.

Withania somnifera Dunal (Solanaceae) or Ashwagandha is also known as "Indian ginseng" has been used for centuries as a nerve tonic and nootropic agent in the Ayurvedic and indigenous systems of medicine [179]. It has been reported that plant preparation such as root

and leaves extracts have neuroprotective roles in ischemic stroke [180][181], Alzheimer's disease [182], pentylenetetrazol seizure [183], Glutamate-Induced Excitotoxicity [184], Huntington's disease [185], and Parkinson's disease [186]. However, until now, none of the studies reported that there is a possibility of neuroprotection by phytochemicals present in *Withania somnifera* through inhibition of NMDAR, gelatinases, nNOS and iNOS at the molecular level. Therefore, present in silico study was designed to elucidate whether *Withania somnifera* phytochemicals inhibit these molecular mediators or not by binding to their active/catalytic domain as similar to their potent inhibitors.

3.2 COMPUTATIONAL METHODS

3.2.1 Retrieval of target protein structures

Atomic coordinates for the 3D structures of GluN2B subunit-containing NMDA receptor, MMP-2, MMP-9 and three isoforms of human NOS, nNOS, eNOS and iNOS were downloaded from RCSB-Protein Data Bank (PDB). Table 3.1 presents the PDB-ID and structural information of each protein. The amino terminal domains of the NMDA glutamate receptor comprises subunit GluN1 (residues 23-405) from *Xenopus laevis* that contain Chain A and C whereas NMDR subunit GluN2B (residues 31-394) from *Rattus norvegicus* consist of Chain B and D. The Ifenprodil inhibitor binds at the GluN1 and GluN2B ATDs heterodimer interface (Fig. 3.2). Structures of three isoforms of human NOS chain B shown in Fig. 3.5 consist of an N-terminal catalytic oxygenase domain comprising a protoporphyrin IX containing Fe (heme) active site and a cofactor site for H4B and C-terminal reductase domain. Figure 3.6 presenting the structures of the catalytic domain of MMP-2 and MMP-9.

3.2.2 Selection and retrieval of structure of WS phytochemicals and inhibitors of target proteins

Phytochemicals present in leaves, root, and shoots of the *Withania somnifera* were listed with the help of kinds of literature [187][188], USDA Phytochemical and Ethnobotanical Databases [189] and NCBI PubChem compounds database [190]. Further, the 3D structure of 40 WS phytochemicals and inhibitors of target proteins were downloaded from RCSB-Protein Data Bank [191] in .sdf format.

Table 3.1: Structural information of molecular targets

Target Name	PDB ID	Structure determination method	Expression system	Resolution	Chains	Deposited by (Reference)
NMDAR	3QEL	X-ray diffraction	*Trichoplusia ni*	2.60 Å	A,B,C,D	[153]
MMP-2	1HOV	NMR spectroscopy	*Escherichia coli*	-	A	[192]
MMP-9	1GKC	X-ray diffraction	*Escherichia coli*	2.3 Å	A, B	[193]
nNOS	4D1N	X-ray diffraction	*Escherichia coli*	2.03 Å	A,B,C,D	[194]
iNOS	4CX7	X-ray diffraction	*Escherichia coli*	3.16 Å	A,B,C,D	[195]
eNOS	4D1O	X-ray diffraction	*Escherichia coli*	1.819 Å	A,B	[194]

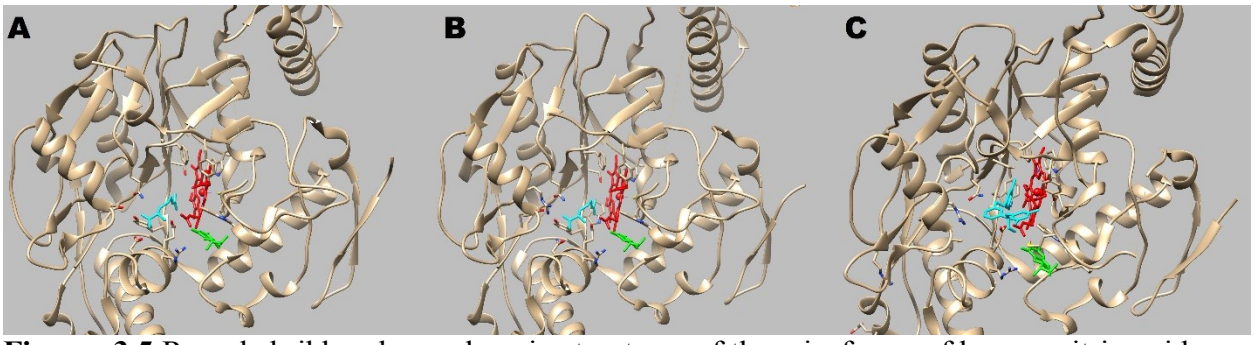

Figure: 3.5 Rounded ribbon heme domain structures of three isoforms of human nitric oxide synthase (Chain B) downloaded from PDB and used for the present study. (A) nNOS (PDB id: 4D1N) (B) eNOS (PDB id: 4D1O) (C) iNOS (PDB id: 4CX7). Substrate L-Arginine (A & B) and S71 inhibitor (C) presented in cyan, Tetrahydrobiopterin (H4B) in green and Protoporphyrin IX Containing Fe (heme) in red color. (Visualization using UCSF Chimera).

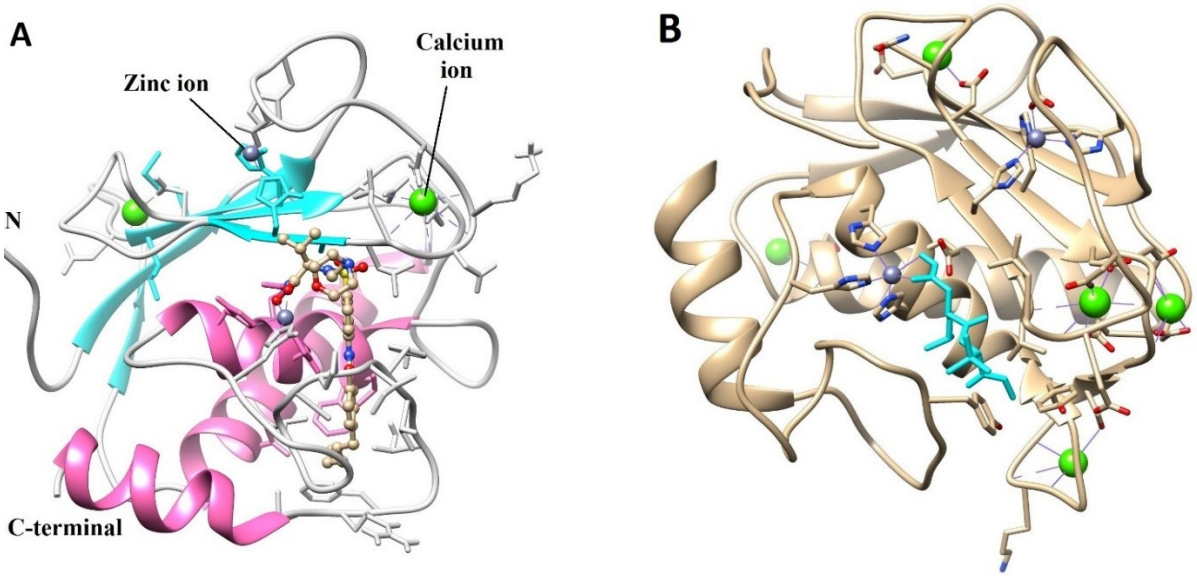

Figure 3.6: MMP-2 and MMP-9 catalytic domain with inhibitors. (A) Ribbon backbone of MMP-2 with five β-strands in cyan and three α-helix in pink as well as ball & stick structure of reverse hydroxamate inhibitor colored by the heteroatom. The active site pocket of MMP-2 contains two zinc ions (blue) and two calcium ions (green). (B) Ribbon backbone of MMP-9 consists of five β-strands, three α-helix and the active site pocket containing zinc ions (blue) and calcium ions (green). The reverse hydroxamate inhibitor (in cyan color) bound in the S1'-the pocket of MMP-9. (Visualization with the UCSF Chimera package v.1.10.2)

3.2.3 Ligands drug properties prediction

WS phytochemicals were examined for their molecular drug properties such as drug-likeness (Lipinski's Rule of Five), Human Intestinal Absorption (HIA), mutagenicity (Ames test) and blood-brain barrier (BBB) penetration. PreADMET server [196] examined mutagenicity and HIA properties of compounds whereas, drug-likeness prediction performed by Lipinski Filters tool [197]. The analysis for blood-brain barrier penetration ability of WS phytochemicals carried out by using online BBB prediction server with the AdaBoost algorithm and PubChem fingerprint (https://www.cbligand.org/BBB/)**.**

3.2.4 Docking preparation for ligands and protein targets

The PyRx-Python prescription 0.8 [198] performed ligands energy minimization by applying mmff94 force field and conjugate gradients optimization algorithm for 200 steps. The structures of NMDAR, nNOS, iNOS, MMP-2 and MMP-9 were prepared and energy

minimized for docking with the help of UCSF Chimera [199]. Protein model was cleaned and optimized by removing ligands as well other heteroatoms. The bulkier structure of NMDAR ATD divided into two separate .pdb files containing Chain A, B and Chain C, D. Chain A, C, and D of nNOS and iNOS, as well as Chain A of eNOS, was removed from their crystal structures. Chain B of three NOSs was saved in .pdb files for further refinement and study. Ligands such as Acetate ion, Sulfate ion, Zinc ion, Glycerol, Gadolinium atom, Bis-Tris Buffer, Arginine, S71-inhibitor and water molecules were removed from the Chain B. The solution structure of MMP-2 contains eleven structures of chain A. We removed ten structures of chain A, and one chain was selected for refinement by removals of hydroxamic acid as well other heteroatoms such as calcium ions and water molecules. As well, from the crystal structure of the MMP-9, chain B, reverse hydroxamate inhibitor, water molecules and calcium ions were removed and chain A was kept for docking studies. Further, deletion of solvent and addition of hydrogens were performed. Charges are added to standard residues (AMBERff14SB) and other residues (AM1-BCC) and are computed using ANTECHAMBER [200]. Subsequently, energy minimization performed for all protein structures by steepest descent method with 100 steps (step size 0.02Å) and conjugate gradient method with ten steps (step size 0.02Å).

3.2.5 Molecular Docking steps

Auto Dock Tools 1.5.6 (ADT) [201] performed docking experiments for the protein tragets and ligands. Kollman charges and Gestgeiger charges were added to each protein structure. Gestgeiger partial charges assigned after merging nonpolar hydrogen and torsions applied to the ligands by rotating all rotatable bonds. Grid box which covers the entire binding site of catalytic or active site domain and hydrophobic pocket as well as provides enough space for the ligands rotational and translational walk were generated for all protein target structures.

Table 3.2 presents grid box parameters for NMDAR, nNOS, iNOS, eNOS, MMP-2 and MMP-9. Rigid docking was performed by using the Lamarckian genetic algorithm (LGA) search parameters with 30 independent runs, 150 population size, 27000 maximum number of generations, 2500000 maximum number of energy evaluations. The rate of gene mutation, the rate of crossover, number of top individuals to survive to next generation (elitism) were default parameters i.e. 0.02, 0.8 and 1 respectively for all protein targets.

Table 3.2 Grid box parameters of protein targets

Target Name	**Grid box parameters**		
	Number of points in X, Y, and Z dimension	Values for grid center for X, Y and Z coordinates	Spacing
NMDA receptor AB Chain (heterodimer)	90, 72 and 98	84.598, 4.492 and -16.127	0.375 A˚
MMP-2 Chain A	80, 80 and 80	4.656, 16.977 and 13.903	0.375 A˚
MMP-9 Chain A	80, 80 and 80	59.039, 23.888 and 116.225	0.375 A˚
nNOS Chain B	100, 80, and 110	center on macromolecule	0.375 A˚
iNOS Chain B	100, 80, and 110	center on macromolecule	0.375 A˚
eNOS Chain B	100, 80, and 110	center on macromolecule	0.375 A˚

3.2.6 Validation of docking accuracy

The accuracy of AutoDock 4.2 docking setup was validated by docking respective inhibitors with NMDAR, nNOS, iNOS, MMP-2 and MMP-9 by keeping same grid and docking parameters mentioned above.

3.3 RESULTS

3.3.1 Drug properties assessment of WS phytochemicals

All compounds assessed against the Lipinski's Rule of Five (LRo5) that distinguishes between a drug like and non-drug like molecules [202]. To be a successful drug, the drug candidate should fall within the following criteria: (a) Molecular mass should be ≤ 500 Dalton, (b) Number of HBD should be ≤ 5, (c) Number of HBA must be ≤ 10, (d) High lipophilicity (LogP

value) should be ≤ 5 [203]. The drug molecules violating two or more of the above rules have less probability of progressing through drug development [204]. These four criteria called the rule of five (Ro5) because all numbers are multiples of five. This Ro5 became a commonly used way of assessing the potential of a compound as a medicinal drug. However, additional features that increase drug-likeness including polar surface area ≤140 $Å^2$ and Molar refractivity should be between 40-130. This rule associated with 90% of orally active drugs that have achieved phase II clinical status; apply only to absorption by passive diffusion of compounds through cell membranes but non-applicable for those compounds that actively transported through cell membranes by transporter proteins [205]. The medicinal chemists widely used this rule to predict the absorption of compounds as well as overall drug-likeness. The BBB is a major obstacle to the delivery of drugs to the central nervous system (CNS). Substances cross the BBB by a variety of mechanisms including transmembrane diffusion, saturable transporters, extracellular pathways and the adsorptive endocytosis [206]. The blood-brain barrier (BBB) prediction server maintained by Xiang-Qun (Sean) Xie's laboratory was used to predict that a compound can pass the BBB (BBB+) or cannot pass the BBB (BBB-) using AdaBoost algorithm with PubChem fingerprint**.** Moreover, prediction of percentage human intestinal absorption (% HIA) helps to design, optimization, and selection of drug candidates for development as oral drugs. The absorption of a drug compound through the human intestinal cell lining is an essential property for potential oral drug candidates [207]. The Ames test is a method to test mutagenicity of a compound as suggested by Dr. Ames [208]. Mutagenicity is the ability of a compound to cause genotoxicity. Experimentally, Ames test performed on *Salmonella typhimurium* bacterial strains where each bacterial strain is sensitive to specific chemical mutagen. However, the development of *in-silico* models as an alternative

approach for mutagenicity assessment of compounds without animal testing is consistently attracting researchers in the field of Quantitative Biological Activity Relationship (QBAR) and toxicology.

Out of 40 listed WS phytochemicals, 25 were selected for the study based on their BBB penetration ability and suitability for Lipinski's Rule of Five. These phytochemicals include 15 steroids (Withanolide-B, Withanolide-G Withanolide M/N/O/P/Q, Withaphysalin F, Withaphysalin M/N/O, Withacnistin, Beta-Sitosterol, Stigmasterol, and Withaferin A) 09 alkaloids (Anahygrine, Somniferine, Tropine, Anaferine, Withasomnine, Chlorogenic Acid, Cuscohygrine, Pelletierine and Calystegine B2) and a Galactitol (dulcitol). All steroids predicted as non-mutagen, and their HIA ranges from 71-100%. Whereas, all non-steroidal compounds predicted as mutagen except Somniferine, which is non-mutagen and their HIA lies between 12-100%. Withanone, Withanolide-A, C, D, E, F, J, R, S, Withaperuvin, Withafastuosin E, scopoletin and Physagulin D were predicted as BBB- (cannot pass the BBB) while other phytochemicals can pass the BBB and predicted as BBB+. Table 3.3 presents the molecular drug properties of forty WS phytochemicals.

Table 3.3 Molecular drug properties of WS phytochemicals.

SN	PubChem CID	Phytochemicals	Lipinski's Rule of Five	% HIA	Mutagenicity	BBB Penetration
1	21679027	Withanone	Suitable	94.740	Non-mutagen	BBB-
2	265237	Withaferin A	Suitable	94.740	Non-mutagen	BBB+
3	11294368	Withanolide A	Suitable	94.740	Non-mutagen	BBB-
4	14236711	Withanolide B	Suitable	96.650	Non-mutagen	BBB+
5	101559583	Withanolide C	Suitable	88.359	Non-mutagen	BBB-
6	161671	Withanolide D	Suitable	94.739	Non-mutagen	BBB-
7	301751	Withanolide E	Suitable	90.403	Non-mutagen	BBB-
8	44562999	withanolide F	Suitable	91.640	Non-mutagen	BBB-
9	21679023	Withanolide G	Suitable	94.478	Non-mutagen	BBB+

10	21679022	Withanolide J	Suitable	91.640	Non-mutagen	BBB-
11	25090669	Withanolide M	Suitable	94.892	Non-mutagen	BBB+
12	23266147	withanolide N	Suitable	94.595	Non-mutagen	BBB+
13	23266146	Withanolide O	Suitable	94.592	Non-mutagen	BBB+
14	21679034	Withanolide P	Suitable	94.478	Non-mutagen	BBB+
15	101281365	Withanolide Q	Suitable	91.644	Non-mutagen	BBB+
16	101281364	Withanolide R	Suitable	94.739	Non-mutagen	BBB-
17	11049407	Withanolide S	Suitable	71.684	Non-mutagen	BBB-
18	44566968	Withaphysalin F	Suitable	94.540	Non-mutagen	BBB+
19	10096775	Withaphysalin M	Suitable	96.885	Non-mutagen	BBB+
20	11752064	Withaphysalin N	Suitable	96.340	Non-mutagen	BBB+
21	10436447	Withaphysalin O	Suitable	97.525	Non-mutagen	BBB+
22	54606507	Withacnistin	Suitable	97.473	Non-mutagen	BBB+
23	222284	Beta-Sitosterol	Suitable	100.000	Non-mutagen	BBB+
24	5280794	Stigmasterol	Suitable	100.000	Non-mutagen	BBB+
25	333470	Withaperuvin	Not-Suitable	50.00	Non-mutagen	BBB-
26	387980	Withafastuosin E	Suitable	84.858	Non-mutagen	BBB-
27	443143	Anaferine	Suitable	90.023	mutagen	BBB+
28	12306778	Anahygrine	Suitable	94.969	mutagen	BBB+
29	14106343	Somniferine	Suitable	95.975	Non-mutagen	BBB+
30	5280460	scopoletin	Suitable	93.924	mutagen	BBB-
31	11850	dulcitol	Suitable	12.812	mutagen	BBB+
32	449293	Tropine	Suitable	99.457	mutagen	BBB+
33	442877	Withasomnine	Suitable	100.000	mutagen	BBB+
34	1794427	Chlorogenic Acid	Suitable	20.427	mutagen	BBB+
35	441070	Cuscohygrine	Suitable	100.000	mutagen	BBB+
36	92987	Pelletierine	Suitable	94.193	mutagen	BBB+
37	124434	Calystegine B2	Suitable	36.118	mutagen	BBB+
38	101689889	Stigmasterol 3-O-beta-D-glucoside	Not-Suitable	90.57	Non-mutagen	BBB+
39	10100412	Physagulin D	Not-Suitable	67.04	Non-mutagen	BBB-
40	5742590	Daucosterol	Not-Suitable	90.03	Non-mutagen	BBB-

3.3.2 Binding mode analysis of Ligands

- **NMDAR-ligand binding analysis**

The ligands were docked at the interface between heterodimers of NMDAR's Chain AB and Chain CD to predict the binding interactions. Comparative study for the mean of the lowest binding energy of all ligands indicated that out of 25 phytochemicals none of them bound to NMDAR with lowest binding energy compared to Ifenprodil (-10.81 kcal/mol). However, ten WS phytochemicals (Anaferine, Beta-Sitosterol, Calystegine B2, Chlorogenic Acid, Cuscohygrine, dulcitol, Pelletierine, Tropine, Withaferin A, Withanolide B) were bound to the dimer interface similar to the Ifenprodil as shown in Fig 3.2. Table 3.4 presents summarizes the results of molecular docking studies comprising lowest binding energy, inhibition constant and NMDAR residues involved in hydrogen bonding (30 docking runs) with these ten phytochemicals and ifenprodil inhibitor.

Table 3.4: Molecular docking results of screened ligands

SN	Ligands	NMDA Receptor Chain (hetero-dimer)	Lowest Binding Energy (kcal/mol)	Estimated Inhibition Constant, Ki	Residues in H-bonding
	NMDAR Inhibitor				
1	Ifenprodil	AB	-10.76	12.89 nM	A:SER108; A:LEU135; B:GLN110
		CD	-10.86	11.04 nM	C:SER108
	WS Phytochemicals				
2	Withaferin A	AB	-9.96	50.34 nM	A:ILE133, A:LEU135
		CD	-9.32	148.01 nM	D:GLU236, C:ARG115
3	Withanolide B	AB	-10.01	45.71 nM	A: ARG115
		CD	-10.31	27.73 nM	C:ARG115
4	Beta-Sitosterol	AB	-9.78	68.08 nM	A:THR333
		CD	-8.78	365.79 nM	C:ASN321

5	Tropine	AB	-5.96	42.72 uM	B:GLY178, B:GLN180
		CD	-6.70	12.30 uM	D:ASP354, D:LYS137
6	Anaferine	AB	-9.12	207.86 nM	B:GLN110, A:SER132
		CD	-11.12	7.02 nM	D:ASP181, D:ASP354
7	Chlorogenic Acid	AB	-7.76	4.07 uM	B:GLN110, A:LEU135, A:ILE133
		CD	-8.16	1.80 uM	D:GLN110, C:ILE133, C:LEU135
8	Cuscohygrine	AB	-7.72	2.19 uM	A:ILE133, B:GLN110
		CD	-8.49	598.34 nM	D:LYS137
9	Pelletierine	AB	-7.13	5.98 uM	B:TYR175, B:MET207, B:GLU236
		CD	-7.25	4.87 uM	D:TYR175, D:MET207
10	Calystegine B2	AB	-6.36	21.84 uM	B:GLN180, B:ASP136, B:GLY178, B:ASP181
		CD	-7.95	1.49 uM	D:ASP354, D:LYS137, D:ASP136
11	dulcitol	AB	-3.98	1.22 mM	A:SER132, B:GLU236, B:GLN110
		CD	-4.01	1.15 mM	C:ASP130, C:SER132,D:ASP181, D:GLN180

- **MMP2-ligand binding analysis**

All ligands including inhibitor and phytochemicals were docked at the S1'-pocket of the catalytic domain of MMP-2 to predict the possible binding interactions between them. Molecular docking results indicated that 19 out of 25 WS phytochemicals have the higher

affinity for MMP-2 due to bind with the lowest energy (< -7.72 kcal/mol) than hydroxamic acid inhibitor. These phytochemicals include all steroids (2-16) and four non-steroids i.e. alkaloids (chlorogenic acid, somniferine, anaferine, and anahygrine). Table 3.5 summarizes the results of molecular docking studies including lowest binding energy, inhibition constant (Ki) and MMP-2 amino acids involved in hydrogen bonding (30 docking runs) with these phytochemicals and hydroxamate inhibitor.

Table 3.5 Docking results of tested ligands against MMP-2

S.N.	Ligands	Lowest Binding Energy (kcal/mol)	Estimated Inhibition Constant (Ki)	**MMP-2 amino acids in H-bonding with ligand (Residues critical in mediating inhibition as reported by Feng et al. [36] indicated in bold)**
Inhibitor of MMP-2				
1	Hydroxamic acid	-7.60	2.66 µM	**Leu83**, **Ala84**, Gly81, **Ala86**, His130, **Glu121**, Glu129, **Leu150**, **Phe148**, Asp45, **Arg38**
***W.somnifera* Phytochemicals**				
2	Withaferin A	-10.03	44.66 nM	Ala136, Thr143, His124, Glu129, **Val117**, Asp72, **Leu83**
3	Withanolide B	-10.38	24.59 nM	**Ala86**, Thr143, **Leu83**, **Arg38**, **Phe148**, **Leu150**
4	Withanolide G	-11.10	7.26 nM	**Leu83**, **Ala84**, Thr143, Ala139, **Glu121**, Gly81, **Phe148**, Asp45, **Arg38**
5	Withanolide M	-10.80	12.13 nM	**Leu83**, Thr143, Ala139, **Ala84**, **Glu121**, **Ala86**, His124, Asp72, His85, **Arg38**, **Phe148**
6	withanolide N	-9.91	54.64 nM	**Leu83**, **Ala84**, **Leu116**, Thr143, His124, Glu129, **Glu121**, Gly81, Tyr142, ASP72, **Arg38**, Gln41, Arg149, Asp45, **Leu150**
7	Withanolide O	-9.45	118.95 nM	**Leu83**, **Ala84**, Gly81, **Ala86**, **Glu121**, His130, Glu129, Ala139
8	Withanolide P	-8.94	277.50 nM	**Ala84**, **Leu83**, Gly81
9	Withanolide Q	-8.93	285.88 nM	**Ala86**, **Glu121**, Ala139, Gly81, **Leu83**, **Ala84**, Asp72, Asp45, **Leu150**, **Arg38**
10	Withaphysalin F	-9.78	68.31 nM	**Ala84**, **Leu83**, His124, **Glu121**, Glu129, **Arg38**

11	Withaphysalin M	-10.41	23.22 nM	Glu129, His124, **Ala84**, **Leu83**, **Arg38**
12	Withaphysalin N	-10.36	25.42 nM	His124, **Ala84**, **Leu83**, Glu129, Asp72, Gln41, **Arg38**
13	Withaphysalin O	-9.59	93.62 nM	Glu129, **Leu83**, His124, Gly81
14	Withacnistin	-9.63	87.55 nM	**Leu83**, **Ala84**, **Arg38**
15	Beta-Sitosterol	-9.32	146.58 nM	Asp72, Tyr74, **Val117**, **Ile141**, **Ala86**, Thr108, Asp45, Asn147
16	Stigmasterol	-9.77	68.56 nM	**Val117**, **Ile141**, Asp72, Tyr74, Thr145, Thr108
17	Somniferine	-10.58	17.67 nM	**Leu83**, **Glu121**, Gly81, **Ala86**, Pro140, **Ala84**, **Phe148**, ASP45, **Leu150**, **Arg38**, Arg149
18	Anaferine	-8.58	517.68 nM	**Ala84**, **Leu83**, **Glu121**, Gly81
19	Chlorogenic Acid	-7.72	2.20 µM	Arg149, Asn147, Lys146, Ala139, Ala136, **Leu83**, Gly81, **Ala84**, Thr143, **Ile141**, **Glu121**, **Ala86**, Tyr142, Tyr74, Tyr144
20	Anahygrine	-7.84	1.78 µM	**Leu83**, **Ala84**, **Glu121**, Gly81, Asp45

- **MMP9-ligand binding analysis**

To predict the possible binding interactions between the WS phytochemicals and MMP-9, all the ligands were docked at the S1'-specificity pocket. Docking was performed with Reverse Hydroxamate Inhibitor and MMP-9 to validate the accuracy of docking setup by keeping same parameters mentioned above. Molecular docking results of screened ligands against MMP-9 indicated that out of 25 phytochemicals 23 molecules have the highest affinity for MMP-9 owing to, they bind with the lowest energy as compare to reverse hydroxamate inhibitor (-7.35 kcal/mol). Table 3.6 summarizes the results of molecular docking studies comprising lowest binding energy, inhibition constant and MMP-9 residues involved in hydrogen bonding (30 docking runs) with these 23 phytochemicals and reverse hydroxamate inhibitor. All WS phytochemicals were bound in the S1'-specificity pocket of the catalytic domain of human

MMP-9 similar to reverse hydroxamate inhibitor (Fig. 3.6B) except Withaphysalin O and Withasomnine, who did not show interaction with residues of S1'-specificity pocket.

Table 3.6 Molecular docking results of selected ligands against MMP-9

SN	Ligands	Lowest Binding Energy (kcal/mol)	Estimated Inhibition Constant (Ki) in nM	Catalytic domain residues in H-bonding with ligand (Residues critical in mediating inhibition as reported by Rowsell et al. [25] presented in bold)
Inhibitors of MMP-9				
1	Reverse Hydroxamate Inhibitor	-7.35	4120	ALA189, **ALA191**, **LEU188**, **GLY186**, TYR393, **TYR423**, ARG424, **GLU402**, TYR420, **PRO421**
***W. Somnifera* Phytochemicals**				
2	Withaferin A	-12.81	0.41	**LEU188, GLY186, HIS411,** ARG424, GLU111, LEU418, LEU397, MET422, **GLU402**, TYR393
3	Withanolide B	-12.25	1.05	ARG424, **GLY186**, TYR393, **HIS411**
4	Withanolide G	-12.30	0.96	**PRO421, TYR423, LEU188, GLY186**, TYR393, GLU111, **HIS411**
5	Withanolide M	-10.57	17.89	**PRO421**, **GLU402**, TYR393, **TYR423**, **GLY186**, ALA189
6	withanolide N	-11.50	3.71	ARG424, **PRO421**, LEU418, MET422, **GLU402**, **GLY186,** TYR420, TYR393, ALA189
7	Withanolide O	-11.28	5.39	GLU111, **GLY186**, TYR393, **PRO421**, ALA189, **LEU188**
8	Withanolide P	-11.94	1.76	**GLU402**, **PRO421**, ALA189, **TYR423**, **LEU188**, **GLY186**, TYR393
9	Withanolide Q	-9.17	188.37	**PRO421**, **GLU402**, **LEU188, TYR423**, ALA189, GLY213, GLY428, ARG143, **HIS411**, **GLY186**
10	Withaphysalin C	-9.48	113.38	**TYR423**, GLY213, GLY428, **LEU188**
11	Withaphysalin D	-10.96	9.27	**GLY186**, **LEU188**, TYR393, **PRO421**, **TYR423**
12	Withaphysalin F	-11.42	4.25	**PRO421**, GLU111, **LEU188**, **GLY186**, TYR393
13	Withaphysalin M	-11.29	5.32	GLU111, **GLY186**, **LEU188**, TYR393, **TYR423**
14	Withaphysalin N	-11.21	6.04	**LEU188, GLY186, TYR423**, TYR393
15	Withaphysalin O	-9.62	88.82	GLU111

16	Withacnistin	-12.49	0.69	**LEU188**, **GLY186**, TYR393, **HIS411**, PHE110, **TYR423**, **ALA191**, ALA189
17	Beta-Sitosterol	-12.66	0.53	GLU111, **TYR423**, PHE110, **GLU402**
18	Stigmasterol	-12.77	0.44	GLU111, **TYR423**
19	Somniferine	-11.18	6.36	ALA189, **LEU188, GLU402,** HIS401
20	Anaferine	-10.74	13.39	**GLU402**, TYR420, ALA189, **PRO421**
21	Withasomnine	-7.92	1580	ALA417, ARG424
22	Chlorogenic Acid	-9.31	148.77	ALA417, ALA189, **LEU188**, **GLY186**, **TYR423**, ARG424, **GLU402**, MET422, **PRO421**, **ALA191**
23	Cuscohygrine	-9.02	245.98	LEU418, **GLU402**
24	Anahygrine	-9.63	87.62	LEU418, **GLU402**, ALA189, **ALA191**

- **NOS-ligand binding analysis**

To predict the proper binding conformation for 7-Nitroindazole (7-NI) and selected 25 WS phytochemicals, docking was performed into the catalytic site of each NOS. Table 3.7 summarizes the binding energy (BE) and Ki value of 26-screened ligands (including 7-Nitroindazole inhibitor and WS phytochemicals) against NOSes. The preliminary study based on binding energy and Ki shows that all phytochemicals have the lower binding energy for nNOS, iNOS and eNOS than its inhibitor except dulcitol. Further, phytochemicals were analyzed for their selectivity for iNOS and nNOS on the basis of their binding energy. Results suggest that only eight phytochemicals namely Withanolide-M, Withanolide-Q, Withacnistin, Stigmasterol, Anaferine, Chlorogenic Acid, Cuscohygrine, and Anahygrine having lower binding energy for iNOS and nNOS compared to eNOS. Table 3.8 summarizes the selectivity of these eight phytochemicals and 7-NI inhibitor.

Table: 3.7 Binding Energy and Ki value of screened ligands against NOSs

SN	**Ligands**	**eNOS**		**iNOS**		**nNOS**	
nNOS inhibitor		**LBE**	**Ki**	**LBE**	**Ki**	**LBE**	**Ki**
1	7-Nitroindazole	-6.84	9.63 uM	-7.07	6.62 uM	-7.18	5.48 uM
WS Phytochemicals							
2	Withanolide B	-10.66	15.40 nM	-10.66	15.48 nM	-12.20	1.14 nM

3	Withanolide G	-10.81	11.99 nM	-10.69	14.49 nM	-10.78	12.58 nM
4	Withanolide M	-10.49	20.50 nM	-11.05	7.94 nM	-10.74	13.42 nM
5	withanolide N	-10.91	10.06 nM	-10.25	30.71 nM	-10.70	14.30 nM
6	Withanolide O	-10.91	10.02 nM	-10.88	10.57 nM	-11.52	3.62 nM
7	Withanolide P	-10.58	17.71 nM	-11.79	2.26 nM	-9.92	53.54 nM
8	Withanolide Q	-10.14	36.69 nM	-10.49	20.31 nM	-11.53	3.54 nM
9	Withaferin A	-10.47	21.16 nM	-9.84	61.24 nM	-10.56	18.13 nM
10	Withaphysalin F	-10.26	30.12 nM	-9.66	82.74 nM	-9.73	73.98 nM
11	Withaphysalin M	-10.98	8.94 nM	-10.16	35.58 nM	-10.74	13.38 nM
12	Withaphysalin N	-10.90	10.26 nM	-10.08	40.72 nM	-10.65	15.63 nM
13	Withaphysalin O	-10.21	33.03 nM	-9.75	71.21 nM	-9.49	111.42nM
14	Withacnistin	-10.38	24.68 nM	-10.49	20.61 nM	-11.17	6.48 nM
15	Beta-Sitosterol	-10.21	32.58 nM	-10.81	11.93 nM	-9.36	137.01 nM
16	Stigmasterol	-9.75	71.68 nM	-11.38	4.56 nM	-10.44	22.34 nM
17	Somniferine	-13.29	182.23 pM	-10.32	27.11 nM	-11.01	8.46 nM
18	Tropine	-7.52	3.07 uM	-7.36	4.04 uM	-7.58	2.78 uM
19	Anaferine	-10.32	27.44 nM	-10.47	21.14 nM	-10.61	16.62 nM
20	Withasomnine	-8.06	1.23 uM	-7.97	1.45 uM	-8.01	1.35 uM
21	Chlorogenic Acid	-6.99	7540 nM	-7.57	2.81 uM	-8.64	463.59nM
22	Cuscohygrine	-8.27	861.37 nM	-8.57	520.49 nM	-8.56	530.15 nM
23	Pelletierine	-7.49	3.21 uM	-7.44	3.51 uM	-7.59	2.74 uM
24	Calystegine B2	-7.36	4.00 uM	-7.27	4.69 uM	-7.64	2.52 uM
25	Anahygrine	-9.24	168.81 nM	-9.35	139.05 nM	-9.62	88.28 nM
26	Dulcitol	-3.12	5.14 mM	-4.21	825.20 uM	-3.90	1.38 mM

Table 3.8 nNOS/iNOS selectivity over eNOS of eight phytochemicals and 7-NI inhibitor

Compounds		**Ki**		**Selectivity over eNOS**	
nNOS inhibitor	**eNOS**	**iNOS**	**nNOS**	**e/i**	**e/n**
7-Nitroindazole	9.63 uM	6.62 uM	5.48 uM	1.45	1.76
***W.somnifera* Phytochemicals**					
Anaferine	27.44 nM	21.14 nM	16.62 nM	1.30	1.65
Anahygrine	168.81 nM	139.05 nM	88.28 nM	1.21	**1.91**
Chlorogenic Acid	7540 nM	2810 nM	463.59nM	**2.68**	**16.26**
Cuscohygrine	861.37 nM	520.49 nM	530.15 nM	**1.65**	1.62
Stigmasterol	71.68 nM	4.56 nM	22.34 nM	**15.72**	**3.2**
Withacnistin	24.68 nM	20.61 nM	6.48 nM	1.20	**3.81**
Withanolide-Q	36.69 nM	20.31 nM	3.54 nM	**1.81**	1.36
Withanolide-M	20.50 nM	7.94 nM	13.42 nM	**2.58**	1.53

Among eight, five phytochemicals (Chlorogenic Acid, Stigmasterol, Cuscohygrine, Withanolide-M, and Withanolide-Q) have shown higher selectivity for nNOS over eNOS (e/n) and four compounds (Chlorogenic Acid, Stigmasterol, Anahygrine, and Withacnistin) have displayed higher selectivity for iNOS over eNOS (e/i) as well as two phytochemicals Chlorogenic Acid and Stigmasterol have shown higher selectivity for both iNOS and nNOS over eNOS (e/i and e/n) compared to 7-NI inhibitor.

3.4 DISCUSSION

- **NMDA inhibition**

The ion-channel activity of NMDARs is allosterically regulated by binding of ifenprodil to the amino-terminal domain (ATD) in a specific manner. Ifenprodil binds at the GluN1-GluN2B subunit interface with insufficient space for entering or exiting through an induced-fit mechanism and it makes hydrophobic interaction with GluN1b, involving LEU 135, TYR 109 and SER 132 as well as interact with GluN2B involving GLU 236, GLN 110 and PHE 176. These residues are critical in mediating allosteric inhibition by ifenprodil reported by Karakas et al. [209]. The chlorogenic acid is a non-steroid compound showed similar binding and interaction as displayed by ifenprodil. It bound to the heterodimer interface with moderate mean binding energy -7.96 kcal/mol with Ki 2.935 μM and exhibited excellent interactions with critical residues of allosteric inhibition reported by Karakas et al. [209]. It was extensively hydrogen bonded to the GluN1b residues LEU135, TYR109 and SER132, also with GluN2B residues GLN110 and GLU23**.** Throughout 30 docking runs, it formed hydrogen bonds with critical residues. When at least 2 hydrogen bonds is considered it established H-bonds 28 times and maximum number of hydrogen bonds was 7! (Higher than ifenprodil). The

LigPlot+(v.1.4.5) presents interaction profile of ifenprodil and chlorogenic acid bound near the interface between heterodimers of NMDAR (Chain AB) shown in Fig 3.7.

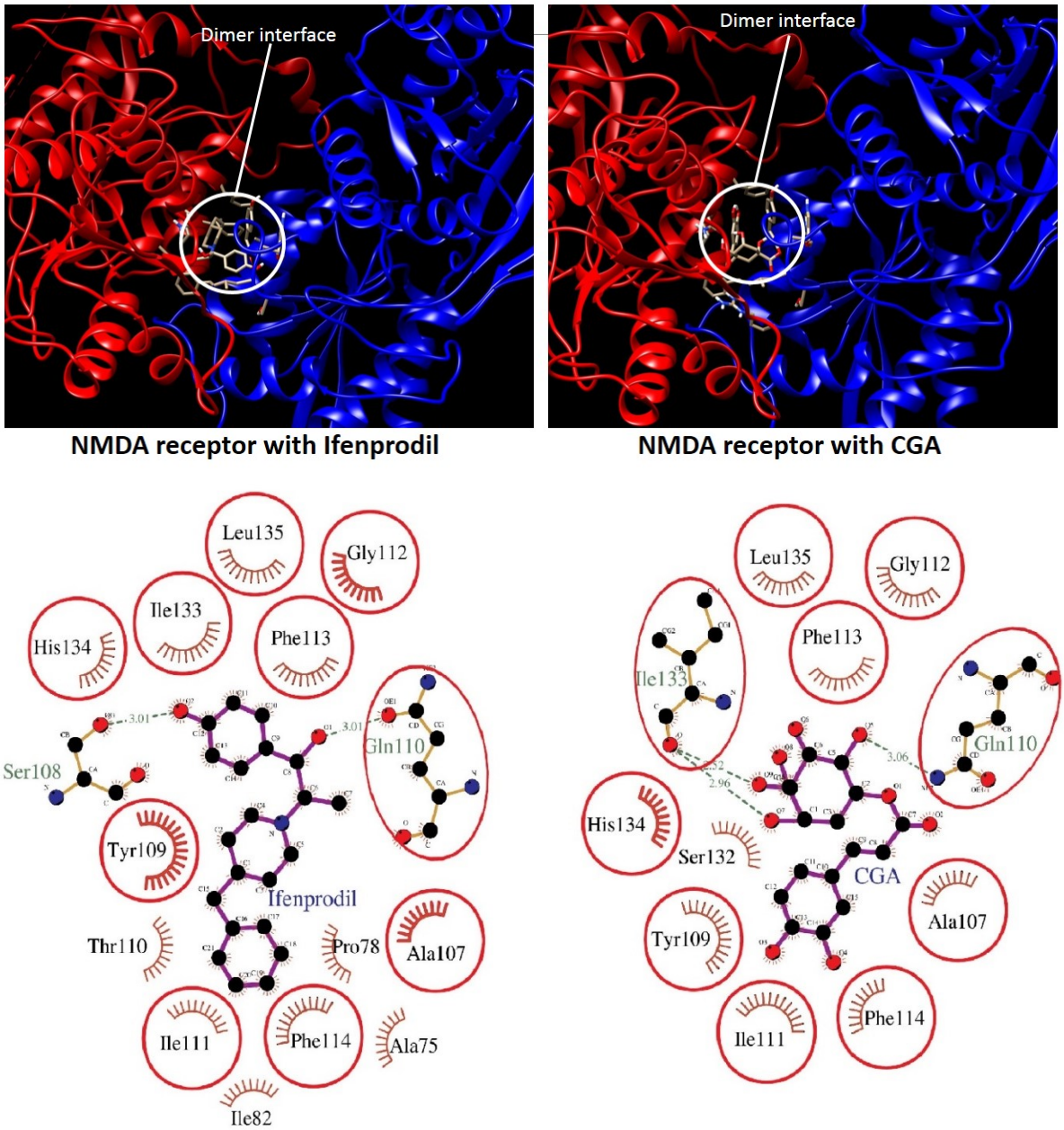

Fig. 3.7: Binding analysis of Ifenprodil and chlorogenic acid at the heterodimer interface of the NMDAR's ATD. (a) Ifenprodil (gray, ball and stick) bound at interface of ATD; (b) CGA (gray, ball and stick) has shown similar binding conformation as displayed by ifenprodil (Visualization using UCSF Chimera). Hydrogen bonding (green dashed lines) and hydrophobic contacts (red arcs with radial spokes) established by ifenprodil (c) and CGA (d) is visualized using LigPlot+ v.1.4.5. The red circles represent the similar residues in H-bonds and hydrophobic contacts established by ifenprodil and CGA with ATD of NMDAR.

- **MMP-2 inhibition**

The MMPs display significant sequence homology and common structural features. The extracellular MMPs consist of a propeptide, a catalytic domain, and a hemopexin-like domain. Moreover, the gelatinases (MMP-2 and MMP-9) contain three fibronectin-like modules within their catalytic domains [192]. After comparing the structure of MMP2 catalytic domain (without fibronectin repeats) and full-length pro-MMP2 it was confirmed that the structure of the catalytic domain is unaffected by the deletion of the fibronectin repeats [193]. There are several subsites (S) present in the MMPs which interact with substrate or inhibitors. The S1'-pocket of the gelatinases offers selective inhibition due to variation in depth and size and has played a significant role in the design of their inhibitors [210].

According to Feng et al. [192], the hydroxamic acid binds in an extended conformation with the isopropyl moiety contacting β-strand IV of the MMP-2 and the large hydrophobic portion filling the S1'-pocket lined with the hydrophobic side-chains of Leu-83, Val-117, Leu-137, Ile-141, Phe-115, and Leu-116. They reported that hydroxamic acid also interacted with Ala-84, His-85, Leu-82, Pro-140, Ala139, Tyr-142, Thr-143, Thr-145, Leu-150, Phe-148, Lys146 and Ala-119 of MMP-2 residues. In the present study, hydroxamic acid bound in the S1'-pocket of the catalytic domain of MMP-2 and involved in hydrogen bonding with Leu-83, Ala-84, Leu-150 as well with the Phe-148, which validated the accuracy of our docking studies. The present docking studies revealed that WS phytochemicals could inhibit MMP-2 catalytic domain by binding at the S1'-pocket similar to the hydroxamic acid with similar interactions at the same site. Among 19 phytochemicals that have lower binding energy than MMP-2 inhibitor, a steroid Withanolide G and an alkaloid Somniferine have shown higher binding energy than all phytochemicals. They bound to the S1'- pocket of the catalytic domain of

human MMP-2 with lowest binding energy -11.10 kcal/mol and -10.58 kcal/mol as well as has smaller inhibition constant (Ki) 7.26 nM and 17.67 nM respectively. The Withanolide G was hydrogen bonded to the Ala-84, Leu-83, Thr-143 and Zn^{2+} ion with bond distances of 3.04, 3.11, 3.13 and 3.06 Å respectively and established hydrophobic contacts with Leu-82, Glu-121, Tyr-74, Gly-81, Val-117, Tyr-142, Leu-116 and Ile-141 residues of the MMP-2 S1'-pocket. The Somniferine was hydrogen bonded to the Pro-140, Ala-84, Glu-121, and Zn^{2+} ion with bond distances of 2.90, 3.18, 2.84 and 3.04 Å respectively and had hydrophobic contacts with Leu-83, Tyr-74, Gly-81, Asp-72, Leu-82 and His-85 residues of the MMP-2 S1'-pocket. Among all phytochemicals the chlorogenic acid showed average binding energy -7.72 kcal/mol with Ki 2.20 µM lower than hydroxamic acid but exhibited great interactions with active site residues of MMP-2. It is involved in hydrogen bonding with Lys-146, Ala-139, Leu-83, Ala-84, Thr-143, Ile-141 and Tyr-142 residues. Fig. 3.8 presents interaction profile of hydroxamic acid and chlorogenic acid with MMP-2.

- **MMP-9 Inhibition**

Among the 26 known MMPs [211], MMP-2, MMP-3, and MMP-9 are widely expressed in the CNS [212]. The catalytic domain of MMP-9 also known as gelatinase B contains zinc-binding site and fibronectin motif repeats that allowing to bind its substrates including components of the ECM, cell adhesion molecules, cell surface receptors, growth factors, cytokines and other proteases. Rowsell et al., 2002 confirmed that the structure of the catalytic domain is unaffected by the deletion of the fibronectin repeats after comparing the structure of MMP-9 catalytic domain (without fibronectin repeats) and full-length pro-MMP-9 [193]. Therefore, the PDB structure of catalytic domain of human MMP-9 (without the fibronectin repeats) determined and submitted by Rowsell et al., was used in present study. This structure consists of a five-

stranded β-sheet and three α-helices and its catalytic center composed of the active-site zinc ion, coordinated by His401, His405 and His411 and an essential Glu402 residue. Rowsell et al. (2002) found that the reverse hydroxamate inhibitor formed hydrogen bonds with Leu188, Leu187, Ala191, Glu402, Gly186, His411, Tyr423 and Pro421 of the MMP-9 catalytic domain [193]. These residues are critical for inhibition of the MMP-9 catalytic domain. The docking study revealed that reverse hydroxamate established H-bonds repeatedly with Ala189, Ala191, Leu188, Gly186, Tyr393, Tyr423, Arg424, Glu402, Tyr420, Pro421 and His411 of the MMP-9 catalytic domain. The residues Ala191, Leu188, Gly186, Tyr423, Glu402, Pro421, and His411, were similar as reported by Rowsell et al. (2002) that validated the accuracy of our docking studies.

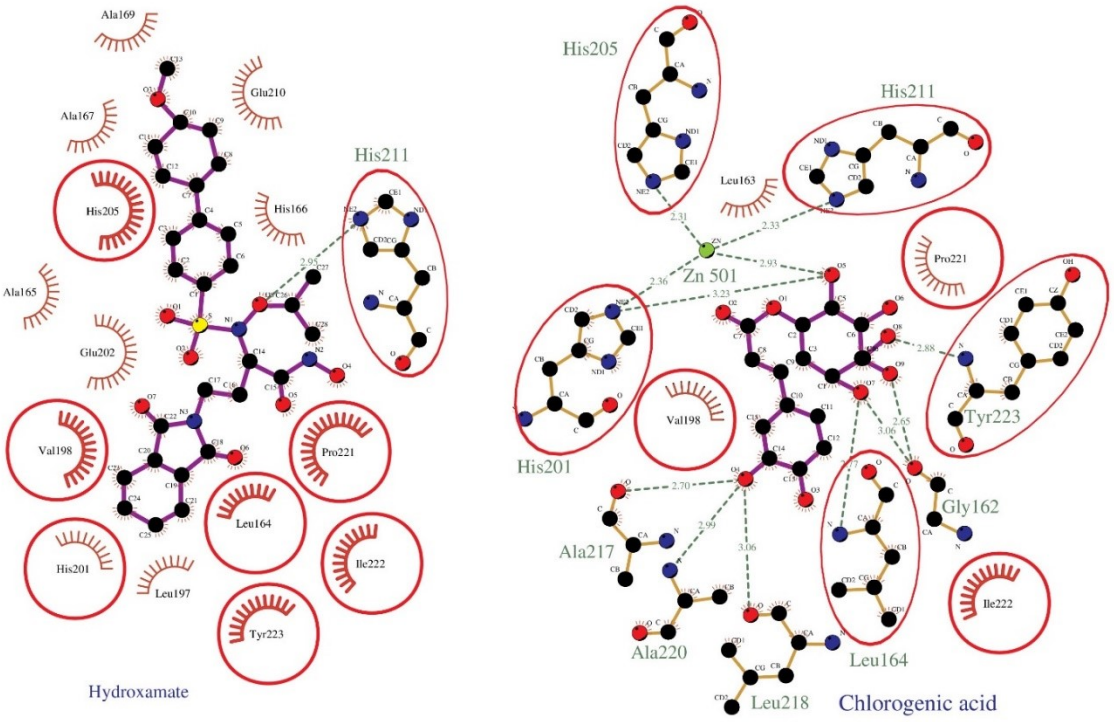

Fig. 3.8 Binding analysis of hydroxamic acid and chlorogenic acid at the S1'-pocket of the catalytic domain of MMP-2. Hydrogen bonding (green dashed lines) and hydrophobic contacts (red arcs with radial spokes) established by ligands is visualized using LigPlot+ v.1.4.5. The red circles represent the similar residues in H-bonds and hydrophobic contacts established by hydroxamic acid and chlorogenic acid with S1'-pocket of the catalytic domain of MMP-2.

Our docking study revealed that Withania somnifera phytochemicals could inhibit MMP-9 catalytic domain by binding to the S1'-specificity pocket similar to the reverse hydroxamate inhibitor Out of 25 phytochemicals, 23 were bound to the active site of the protein with higher affinity in terms of lower binding energy than priors The critical residues for inhibition found in the S1'-specificity pocket of the catalytic domain of MMP-9 specifically Ala191, Glu402, Leu188, Gly186, Pro421 and Tyr423 involved in hydrogen bonding with the reverse hydroxamate inhibitor which validated the accuracy of our docking study. Some residues from these show interactions regarding hydrogen bonding and hydrophobic contacts with 21 *Withania somnifera* phytochemicals whereas, Withaphysalin O and Withasomnine do not interact via hydrogen bond formation with these residues. We further analyzed interaction profile of two compounds that exhibit higher affinity toward MMP-9, a steroidal compound Withaferin A and an alkaloid Somniferine. The Withaferin A was hydrogen bonded to the Leu188, Gly186 and His411 with bond distances of 3.04, 2.50 and 3.03 Å respectively and established hydrophobic contacts with Ala189, His401, His405, Leu187, Glu402, Phe110, His190, Glu111, Pro421, Tyr423 and Met422 residues of the MMP-9. The Somniferine was hydrogen bonded to the His401, Glu402 and Zn2+ ion with bond distances of 1.85, 2.92 and 2.39 Å respectively and had hydrophobic contacts with Phe110, Ala189, Tyr179, His190, Val398, Pro421, Leu188, Leu187 and Gly186 residues of the MMP-9. Among all phytochemicals chlorogenic acid formed higher number of H-bonding and established hydrophobic interaction with MMP-9 in each docking run. Fig. 3.9 illustrates the binding interaction of MMP-9 inhibitor and chlorogenic acid with catalytic domain of MMP-9.

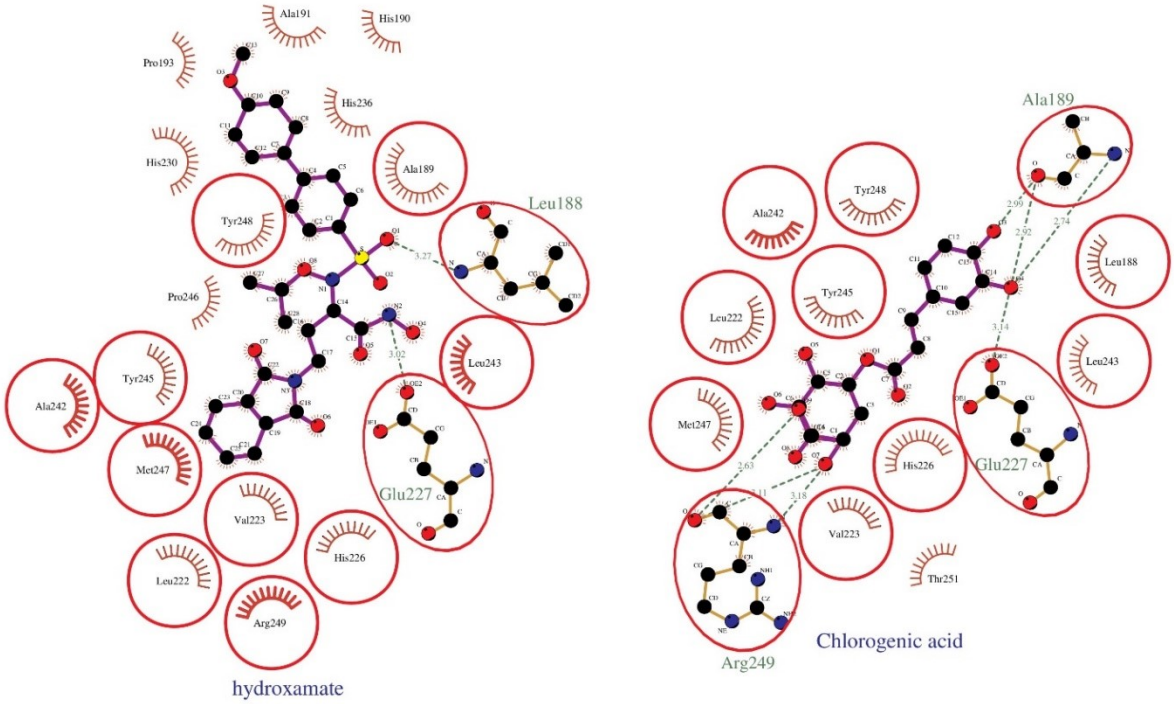

Fig. 3.9 Binding analysis of reverse hydroxamic acid and chlorogenic acid at the S1'-pocket of the catalytic domain of MMP-9. Hydrogen bonding (green dashed lines) and hydrophobic contacts (red arcs with radial spokes) established by ligands is visualized using LigPlot+ v.1.4.5. The red circles represent the similar residues in H-bonds and hydrophobic contacts established by reverse hydroxamic acid and chlorogenic acid with S1'-pocket of the catalytic domain of MMP-9.

- **Selective dual inhibition of nNOS and iNOS over eNOS**

When 7-NI, a selective inhibitor of nNOS [213] was docked into the catalytic domain of rat nNOS, it bound to the heme domain (Fig. 3.5) and formed hydrogen bonding with Glu597, Tyr593, Gln483, Trp592, Hem750, Asp602, Gln483, Pro570, Phe589, Tyr711, Asn574, and Phe709 residues in 30 docking runs. It formed H-bonds with Trp372, Arg388, Glu494, Glu377, Tyr373, Hem550, and Asn354 residues of hem domain of iNOS. It is evident that among all, the Chlorogenic Acid showed the highest nNOS selectivity and with estimated free energy of binding (-8.64 kcal/mol) and estimated inhibition constant, Ki (463.59 nM). Chlorogenic Acid forms nine H-bonds with Asp602, Arg608, Arg486, Gln483, Tyr593, Val572, Pro570 and

Phe589 residues and establishes five hydrophobic interactions with Glu597, Ala571, Arg601, Hem750 and Ser590 residues of nNOS catalytic domain. It forms five hydrogen bonds and eight hydrophobic interaction with eNOS as well as forms six hydrogen bonds and eight hydrophobic interaction with iNOS. Fig. 3.10 presents the binding pattern of chlorogenic acid with three isoform of NOSes.

On the basis of lower binding energy, lower Ki value, higher H-bonds formation, suitability for Lipinski's Rule of Five we can say that Chlorogenic Acid, and stigmasterol can inhibit nNOS and iNOS selectively over eNOS and have a potential to be developed as a dual inhibitor of nNOS and iNOS.

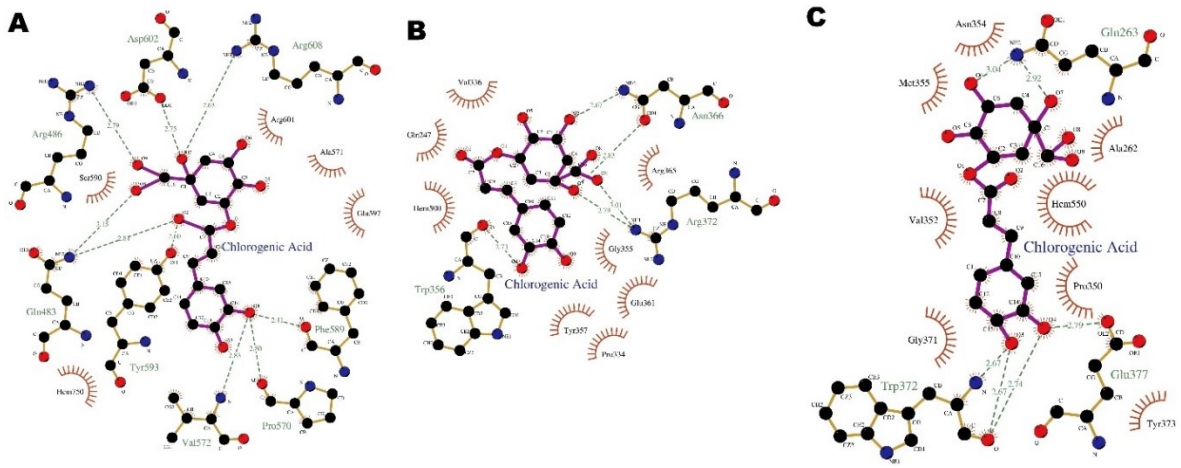

Figure: 3.10 Hydrogen bonding and hydrophobic interactions of Chlorogenic Acid with (A) nNOS (B) eNOS and (C) iNOS. (Visualization using LigPlot+ v.1.4.5). Ligand or residue bonds are blue and orange, respectively. Hydrogen bonds are depicted with green dashed lines. The corresponding interatomic distances are indicated. Heme domain residues involved in hydrophobic interactions with the ligands are represented as labeled arcs with radial spokes that point toward the ligand atoms with which they interact.

3.5 CONCLUSION

The present *in silico* study provides significant evidence that WS phytochemicals can inhibit NMDAR, MMP-2, MMP-9, nNOS and iNOS, hence able to confer neuroprotection in the stroke condition. We found that out of forty phytochemicals, 25 compounds of WS qualify all

criteria, as they are found suitable in Lipinski's Rule of Five, able to penetrate BBB and have high Human Intestinal Absorption (HIA). These molecules were docked near the catalytic/active site of five molecular targets namely NMDAR, MMP-2, MMP-9, nNOS and iNOS. Surprisingly, chlorogenic acid appeared as a potent multi-target inhibitor as it displayed extensive hydrogen bounding and hydrophobic interaction with all molecular targets compared to their inhibitors. It also showed higher selectivity for nNOS and iNOS over eNOS. Therefore, we can say that chlorogenic acid as a non-steroidal compound can be developed as a potential neurotherapeutic agents to combat ischemic stroke. Further, its brain penetration and neuroprotective potential will be evaluated *in vivo*.